Carrier Dynamics and Microwave Characteristics of GaAs-Based Quantum-Well Lasers

I. Esquivias, *Member, IEEE*, S. Weisser, B. Romero, J. D. Ralston, *Life Member, IEEE*, and J. Rosenzweig

***Abstract*— We investigate the effects of carrier capture and re-emission on the electrical impedance, equivalent circuit, and modulation response of quantum-well (QW) laser diodes. The electrical impedance is shown to be a sensitive function of the time constants associated with carrier capture/transport and carrier re-emission. We compare the theoretical results with measured values of the electrical impedance of high-speed InGaAs–GaAs multiple-quantum-well lasers fabricated using different epilayer structures with a common lateral structure. The experimental results agree well with the theoretical model, allowing us to extract the effective carrier escape time and the effective carrier lifetime in the QW's, and to estimate the effective carrier capture/transport time.**

***Index Terms*— Equivalent circuit, gallium compounds, impedance measurement, laser measurements, quantum-well lasers, semiconductor lasers.**

I. Introduction

THE MAXIMUM modulation bandwidth that can be achieved using quantum-well (QW) active regions in semiconductor lasers is still the subject of intense debate, both theoretically and experimentally. While it was theoretically predicted that QW lasers could attain substantially higher direct modulation bandwidths than their bulk counterparts [1], [2], it is only recently that direct modulation bandwidths exceeding the record values for InP-based and GaAs-based bulk devices have really been measured [3]–[6]. Electrical parasitics, device or carrier heating, and nonlinear gain can limit the modulation bandwidth of both bulk and QW lasers. However, one problem intrinsic to QW devices is the additional bandwidth limitation arising from the processes of carrier capture into the QW's, carrier escape from the QW's into the core, and carrier transport across the core [7]–[10]. The influenc of these processes on the modulation response and the relative intensity noise (RIN) [11] have been extensively studied using a rate-equation approach. However, the values of the time constants entering into the rate equations describing carrier capture, transport, and re-emission are not well known for practical laser structures. Furthermore, the unambiguous determination of these time constants from measured values of the modulation response or RIN is not possible in general.

Using a rate-equation approach, we have derived the expressions for the electrical impedance of a QW laser [12]. Accurate knowledge of the laser electrical impedance and the laser equivalent circuit is not only required for the design of electronic laser drivers, but is also useful to gain further insight into the laser dynamics, since the electrical impedance is a sensitive function of the time constants describing carrier capture and re-emission. An analysis of the frequency dependence of the subthreshold electrical impedance can provide reasonable estimations for the values of the dynamic time constants. This approach has been applied to extract the escape time and to estimate the capture time for GaAs-based QW lasers with different layer structures and device geometry [12]–[16].

In this paper, we extend the theoretical analysis and present further experimental data to illustrate the dependence of the electrical impedance, the laser equivalent circuit, and the modulation response of strained InGaAs–GaAs lasers on the values of these time constants. The paper is organized as follows. In Section II, we review the rate-equation model used to calculate the modulation response, electrical impedance, and the laser equivalent circuit. In Sections III and IV, we provide analytical expressions for the steady-state and small-signal characteristics, respectively. Simplifie expressions for the impedance, modulation response, and equivalent circuit in some special cases are given in Section V. Section VI presents the results of measurements of the electrical impedance of high-speed laser diodes fabricated using different epilayer structures with a common lateral structure. We demonstrate that the measured values of the impedance versus frequency can be accurately modeled using the simple expressions derived from the rate equations. Three qualitatively different behaviors of the impedance versus frequency are observed, which are predominantly due to different values of the carrier escape time in the different epilayer structures. In this section, we further present the values of the time constants describing the carrier dynamics extracted from these measurements. Finally, we summarize our main results in Section VII.

II. Rate-Equation Model

In order to model the dynamical properties of QW lasers, we use single-particle rate equations describing the dynamics of electron–hole pairs. The more general two-particle models

Manuscript received August 3, 1998; revised December 7, 1998. This work was supported by the Bundesministerium für Bildung, Wissenschaft, Forschung und Technologie (BMBF), Germany, and by the Comisión Interministerial de Ciencia y Tecnología, Spain, under Project TIC95-0563-C05-04.

I. Esquivias and B. Romero are with the Departamento de Tecnología Fotónica, Universidad Politécnica de Madrid, Ciudad Universitaria, E-28040 Madrid, Spain.

S. Weisser and J. Rosenzweig are with the Fraunhofer-Institut für Angewandte Festkörperphysik, D-79108 Freiburg, Germany.

J. D. Ralston was with the Fraunhofer-Institut für Angewandte Festkörperphysik, D-79108 Freiburg, Germany. He is is now with the Management of Technology Program, Massachusetts Institute of Technology, Cambridge, MA 02138 USA.

Publisher Item Identifie S 0018-9197(99)02538-5.

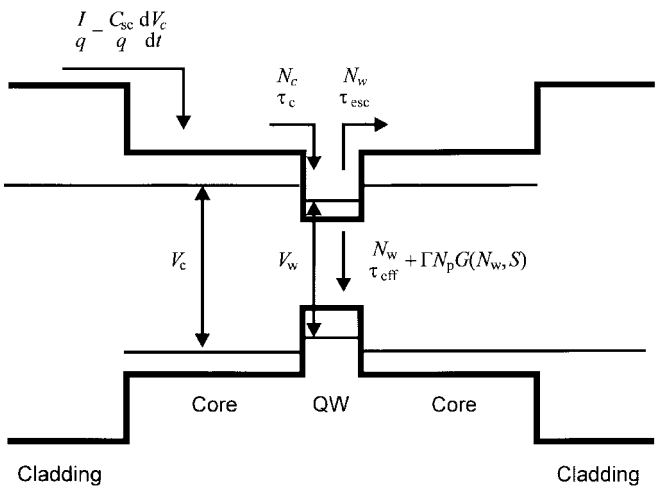

Fig. 1. Schematic diagram of a QW laser structure under flatban conditions including quasi-Fermi levels and carrier capture, re-emission, and recombination processes.

require the analysis of four (or more) nonlinear coupled rate equations [17], for which simple solutions do not exist. However, as will be shown in this paper, this single-particle model accurately describes the measured values of both electrical (differential diode resistance and electrical impedance) properties and the modulation response of the GaAs-based lasers investigated in this study, so that the use of two-particle models is not merited. We assume a homogeneous *vertical* carrier distribution in the total core region (including the barriers between the QW's) and neglect carrier transport effects *between the QW's* in multiple-quantum-well (MQW) lasers [18], resulting in a homogeneous carrier distribution in the QW's. In addition, the lateral carrier distribution in the core and in the QW's is assumed to be homogeneous, neglecting the effects of lateral carrier diffusion [19].

Fig. 1 illustrates the dominant processes in QW lasers. The dynamic behavior of a QW laser is modeled using three rate equations, one each for the photon number in the cavity N_p, the *number* of unconfine carriers N_c, and the *total number* of confine carriers in the QW's N_w. In analogy to the models for bulk lasers [20], we include the influenc of the space-charge capacitance C_{sc} into the rate equations, which, as will be evident from the experimental results in Section VI, is important to explain the dynamical laser properties. Considering the effect of C_{sc}, the net current used to change the amount of charge stored in the core and in the QW's is written as $I–C_{sc} \cdot dV_c/dt$ where I is the total injection current and $C_{sc} \cdot dV_c/dt$ is the current required to change the amount of charge stored in the depletion region of the junction, where V_c is the junction voltage. Carriers are injected into the core from the highly doped cladding layers, building up a population of *unconfine carriers in the core*. The carrier population in the core interacts with the *confine carriers in the QW's* by the processes of *carrier capture* into the QW's (rate N_c/τ_{cap} with the effective capture time τ_{cap}) and *carrier re-emission* from the QW's (rate N_w/τ_{esc} with the effective escape time τ_{esc}). In this analysis, we neglect the recombination of carriers in the core and the re-emission of carriers from the core into the cladding layers. Both effects could be included in the analysis by adding an additional loss rate for carriers in the core to the corresponding rate equation [21]. The carriers in the QW's recombine via *stimulated emission* with the rate $N_p \cdot \Gamma G(N_w, N_p)$, where $G(N_w, N_p)$ is the optical material gain and Γ is the confinemen factor, and by *nonradiative recombination* and *spontaneous emission into all optical modes*. The latter two processes are summarized in the rate N_w/τ_{eff} where τ_{eff} is the effective carrier lifetime in the QW's. The rate equations are thus written as

$$\begin{aligned}
\frac{dN_p}{dt} &= \left[\Gamma G(N_w, N_p) - \frac{1}{\tau_p}\right] \cdot N_p \\
\frac{dN_w}{dt} &= -\left[\frac{1}{\tau_{eff}} + \frac{1}{\tau_{esc}}\right] \cdot N_w + \frac{N_c}{\tau_{cap}} - N_p \cdot \Gamma G(N_w, N_p) \\
\frac{dN_c}{dt} &= \frac{I}{q} - \frac{dV_c}{dt}\frac{C_{sc}}{q} - \frac{N_c}{\tau_{cap}} + \frac{N_w}{\tau_{esc}}
\end{aligned} \tag{1}$$

where τ_p is the photon lifetime and q is the elementary charge.

It is important to note that the physical capture time $\tau_{cap,\,phys}$ is *not* identical to the effective capture time $\tau_{cap} = \tau_{cap,\,phys} \cdot d_c/d_w$ appearing in the rate equations, the latter containing a scale-up factor given by the ratio of the total core thickness d_c and the total QW thickness d_w [22]. *Transport effects* of carriers across the core lead to an inhomogeneous carrier distribution in the core [23]. However, the dynamic properties of QW lasers in the presence of carrier transport effects can also be described by (1), but with the effective carrier capture time replaced by the carrier transport time [7]. In the general case, the *combined effects* of carrier transport and carrier capture can be included in the analysis by using the expression for the effective carrier capture time $\tau_{cap} = \tau_{diff} + \tau_{cap,\,phys} \cdot d_c/d_w$ [22] where τ_{diff} is the carrier diffusion time across the core in (1).

The dependence of the optical material gain on the photon number is phenomenologically described using the nonlinear gain coefficien ε. Throughout this paper, we restrict the analysis to the case of weak gain suppression $\varepsilon S \ll 1$, where the photon density S is given by $S = N_p\Gamma/Ad_w$ (A denotes the active region area), and use the linearized expression

$$G(N_w, N_p) = G_0(N_w) \cdot (1 - \varepsilon \cdot S). \tag{2}$$

For the InGaAs–GaAs lasers investigated in this study, typical values of the nonlinear gain coefficient as determined from RIN measurements, are in the range of $\varepsilon = 4.6–8.6 \times 10^{-17}$ cm^3 [24]. Maximum CW photon densities in these devices are typically $S_{max} \approx 2.5 \times 10^{15}$ cm^{-3}, confirmin the validity of the approximation (2) even at the highest photon densities.

A key step in the derivation of the laser equivalent circuit is to relate the carrier number in the core to the voltage applied across the core, V_c. Numerical calculations considering the whole set of semiconductor equations have shown that the quasi-Fermi levels for the unconfine carriers are fla throughout the core region and that the separation is given by the applied voltage [25]; assuming Boltzmann statistics for the unconfine carriers and neglecting electrical parasitics, the former can be used to express N_c as

$$N_c \propto e^{V_c/mV_T} \quad \text{with} \quad V_T = kT/q \tag{3}$$

where k and T are the Boltzmann constant and the absolute temperature, respectively. The factor m takes a value of one (two) when the injected unconfine carrier density is lower (higher) than the core-doping density.

III. Steady-State Characteristics

The steady-state solution of (1) is obtained by setting the time derivatives to zero. In the following analysis, we assume that $\tau_{\rm eff}$, $\tau_{\rm esc}$, and $\tau_{\rm cap}$ do not depend on the carrier numbers in the core and in the QW's. This assumption is used only to obtain simple expressions with clear physical insight; an analysis of the steady-state characteristics considering the carrier density dependencies of the time constants yields the same qualitative results. The exact solution for the steady-state carrier number in the core N_{c0} is then given as

$$N_{c0} = \eta N_{w0} + \frac{I_0 \tau_{\rm cap}}{q} \tag{4}$$

where I_0 is the bias current, N_{w0} is the steady-state carrier number in the QW's, and $\eta = \tau_{\rm cap}/\tau_{\rm esc}$. As can be seen from (4), η denotes the equilibrium ratio ($I_0 = 0$) of the carrier numbers in the core and in the QW. The value of η is determined by the band structures in the QW's and in the core. In order to obtain satisfactory dynamical performance of the laser, the relation $\eta \ll 1$ must hold (see the discussion in Section V). Under forward bias, the carrier number in the core is larger than the value of ηN_{w0} due to the additional contribution $I_0\tau_{\rm cap}/q$ arising from the finit capture time. In the subthreshold regime ($N_p = 0$), the steady-state carrier numbers are given as

$$N_{w0} = \frac{I_0 \tau_{\rm eff}}{q} \quad \text{and} \quad N_{c0} = \eta \frac{I_0 \tau_{\rm eff}}{q} \cdot \left(1 + \frac{\tau_{\rm esc}}{\tau_{\rm eff}}\right). \tag{5}$$

In the limit $\tau_{\rm esc} \ll \tau_{\rm eff}$, the ratio N_{c0}/N_{w0} is identical to the equilibrium value η, which is the minimum value that can be achieved. In the opposite case $\tau_{\rm esc} \gg \tau_{\rm eff}$, the carrier number in the core is dominated by carrier accumulation due to the finit capture time, yielding a ratio N_{c0}/N_{w0} well above the equilibrium value. Above threshold, the optical material gain *in the absence of nonlinear gain* ($\varepsilon = 0$) is clamped to its threshold value $1/\Gamma\tau_p$, resulting in a clamping of the carrier number in the QW's to $N_{w0} = N_{w\rm th}$. When nonlinear gain is taken into account, the carrier number in the QW's above threshold is slightly larger than the threshold value. For the following calculation of the steady-state properties above threshold, we neglect this small contribution and set $N_{w0} = N_{w\rm th}$. This approximation (perfect gain clamping) is frequently used for the calculation of steady-state properties [26] of bulk lasers. This yields

$$N_{c0} = \eta N_{w\rm th} + \frac{I_o \tau_{\rm cap}}{q} = \tau_{\rm cap} \cdot \frac{I_0 + (\tau_{\rm eff}/\tau_{\rm esc}) \cdot I_{\rm th}}{q} \tag{6}$$

in which the threshold current $I_{\rm th}$ is given by $I_{\rm th} = qN_{\rm th}/\tau_{\rm eff}$. In general, the carrier number in the core increases above threshold with increasing bias current beyond the value $\eta N_{w\rm th}$. The absence of clamping for the unconfine carriers in the core has been experimentally confirme from above-threshold spontaneous emission [17], [27] and differential resistance measurements, on which we will comment later.

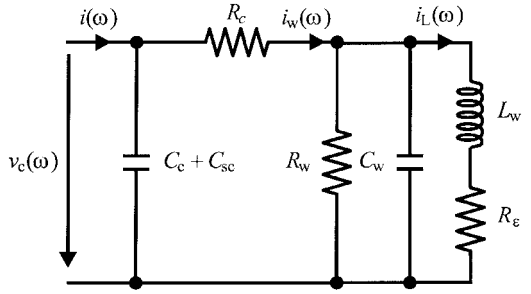

Fig. 2. Small-signal intrinsic equivalent circuit of a QW laser diode.

IV. Small-Signal Characteristics

In the following discussion, we use the small-signal solution of (1) to calculate the laser intrinsic equivalent circuit, intrinsic electrical impedance, and intrinsic modulation response. The intrinsic electrical impedance and the intrinsic equivalent circuit of *bulk* laser diodes have been derived in [28] and [29]. In [30], the intrinsic equivalent circuit of a QW laser considering carrier capture and re-emission has been derived. A similar intrinsic equivalent circuit for QW laser diodes in the presence of carrier transport effects was published in [31]. We follow the analysis in [30] but explicitly include the effect of the space–charge capacitance [12]. The solution of (1) in the small-signal regime is obtained by expanding the variables I, N_p, N_w, and N_c around their steady-state values, e.g., $I(t) = I_0 + i(\omega)\, e^{j\omega t}$. The relation between the small-signal values of the voltage across the core $v_c(\omega)$ and the carrier number in the core $n_c(\omega)$ is obtained by linearization of (3), yielding

$$v_c(\omega) = \frac{q n_c(\omega)}{C_c}, \qquad C_c = \frac{q N_{c0}}{m V_T}. \tag{7}$$

In analogy to (7), we further defin the small-signal voltage related to the separation of the quasi-Fermi levels in the QW's as

$$v_w(\omega) = \frac{q n_w(\omega)}{C_w}, \qquad C_w = \frac{C_c}{\eta}. \tag{8}$$

The capacitances C_c and C_w are associated with the unconfine carriers and with the confine carriers in the QW's, respectively. As shown in the Appendix, the linearization of (1), using (7) and (8) to eliminate $n_c(\omega)$ and $n_w(\omega)$, yields the small-signal intrinsic equivalent circuit of a QW laser diode shown in Fig. 2. The remaining circuit elements are given as

$$\begin{aligned} R_c &= \tau_{\rm cap}/C_c \\ R_w &= \tau_w/C_w, \quad 1/\tau_w = 1/\tau_{\rm eff} + \omega_r^2 \tau_p \\ L_w &= 1/(\omega_r^2 C_w) \\ R_\varepsilon &= \varepsilon/(G_0' C_w) \ \text{ above threshold} \end{aligned} \tag{9}$$

where the differential gain G_0' is given by $G_0' = A d_w \partial G_0/\partial N_w$ and the classical expression for the angular relaxation frequency is $\omega_r = \sqrt{G_0' S_0/\tau_p}$. The time constant τ_w denotes the *total* differential carrier lifetime in the QW's,

summarizng the effects of nonradiative recombination and spontaneous emission into all cavity modes (via $\tau_{\rm eff}$) and of stimulated emission above threshold (via $\omega_r^2\tau_p$). The latter contribution vanishes below threshold, yielding $\tau_w = \tau_{\rm eff}$. Note that the small-signal current $i_L(\omega)$ flowin through the inductance L_w is proportional to the small-signal portion of the emitted stimulated output power above threshold $i_L(\omega) = qn_p(\omega)/\tau_p$. The equivalent circuit shown in Fig. 2 is valid below and above threshold with vanishing elements L_w and R_ϵ below threshold.

The *exact expressions* for the intrinsic impedance $Z_i(\omega) = v_c(\omega)/i(\omega)$ and the normalized intrinsic modulation response $H(\omega) = qn_p(\omega)/\tau_p i(\omega)$ calculated using this equivalent circuit are given by (10), shown at the bottom of the page, where $\gamma_I = 1/\tau_{\rm esc} + \gamma$, and the damping rate and electrical time constant are given, respectively, by

$$\gamma = 1/\tau_{\rm eff} + \omega_r^2(\tau_p + \varepsilon/G_0') \tag{11}$$

$$\tau_0 = \tau_{\rm cap}(1 + C_{\rm sc}/C_c) = \tau_{\rm cap} + R_c C_{\rm sc}. \tag{12}$$

The second equation in (10) is valid above threshold; the expression for the intrinsic impedance below threshold is recovered in the limit $N_{p0} = 0$ (set $\omega_r = 0$ and $\gamma = 1/\tau_{\rm eff}$).

The *intrinsic differential diode resistance* $R_d = Z_i(0)$ is obtained by inspection of the equivalent circuit in Fig. 2 as $R_d = R_c + R_w$ below threshold, and $R_d = R_c + (R_w \| R_\epsilon)$ above threshold, where $\|$ denotes a parallel combination. Using (7)–(9) in conjunction with (5) and (6), we derive the following expressions:

Below threshold:

$$R_c(I_0) = \frac{mV_T}{I_0} \cdot \frac{1}{1 + \dfrac{\tau_{\rm eff}}{\tau_{\rm esc}}} \quad \text{and} \quad R_d(I_0) = \frac{mV_T}{I_0}$$

Above threshold:

$$R_c(I_0) = \frac{mV_T}{I_0 + \dfrac{\tau_{\rm eff}}{\tau_{\rm esc}} I_{th}} \quad \text{and} \quad R_d(I_0) = R_c(I_0) \tag{13}$$

In the expression for R_d above threshold, we have neglected the contribution of R_ϵ and have further assumed perfect gain clamping in the QW's ($N_w = N_{w\rm th}$ above threshold).

V. Simplified Expressions

In general, a simple decomposition of the denominator in (10) into a low-pass filte term and a resonance term containing the relaxation frequency and the damping rate does not exist. In this section, we discuss three special cases, where simple analytical formulas can be derived. Throughout this section, we further assume $\varepsilon/(G'\tau_w) \ll 1$.

We firs consider the case $\eta \ll 1$, which is the case of interest for high-speed laser diodes with deep QW's and narrow confinemen regions. For a finit ratio $C_{\rm sc}/C_c$, the condition $\eta \ll 1$ is equivalent to $\tau_0 \ll \tau_{\rm esc}$. In this case, the modulation response and the intrinsic impedance simplify to

$$H(\omega) = \frac{\omega_r^2\tau_p}{(1 + j\omega\tau_0)(\omega_r^2 - \omega^2 + j\omega\gamma)}$$

and

$$Z_i(\omega) = R_d \cdot \frac{1}{1 + j\omega\tau_0} \cdot T(\omega) \tag{14}$$

where the function $T(\omega)$ is given by

Below threshold:

$$T(\omega) = \frac{1 + j\omega\tau_I}{1 + j\omega\tau_{\rm eff}}$$

Above threshold:

$$T(\omega) = \frac{\omega_r^2 - \omega^2 + j\omega\gamma_I}{\omega_r^2 - \omega^2 + j\omega\gamma} \tag{15}$$

and $1/\tau_I = 1/\tau_{\rm eff} + 1/\tau_{\rm esc}$. In this case, the only influenc on the modulation response is an additional low-pass filte with the time constant τ_0, whereas the expressions for the relaxation frequency and the damping rate are not modifie by the carrier capture/transport and re-emission processes. However, depending on the ratio of $\tau_{\rm eff}$ and $\tau_{\rm esc}$, qualitatively different behaviors of the frequency-dependent impedance are observed, which are schematically plotted in Fig. 3.

1) Case I—$\eta \ll 1$ and $\tau_{\rm esc} \gg \tau_{\rm eff}$: In this case, $T(\omega) = 1$ below and above threshold, and the impedance simplifie to a simple low-pass filte with time constant τ_0, allowing only the extraction of τ_0 from measured curves. The equivalent circuit in this case is shown in Fig. 4(a) with $R_c = mV_T/I_0$ and $R_c C_c = \tau_c$. The intrinsic differential diode resistance (13) simplifie to the corresponding expression for conventional diodes $R_d = mV_T/I_0$, both below and above threshold.

2) Case II—$\eta \ll 1$ and the Same Order of Magnitude of $\tau_{\rm esc}$ and $\tau_{\rm eff}$: Below threshold, two poles at $\tau_{\rm eff}$ and τ_0 and one zero at $(\tau_{\rm eff}^{-1} + \tau_{\rm esc}^{-1})^{-1}$ with significantl different values are observed in the impedance, allowing the extraction of $\tau_{\rm eff}$, $\tau_{\rm esc}$, and τ_0 from measured curves. Above threshold, the impedance exhibits a peak at the relaxation frequency with the relative height $T(\omega_r) = 1 + 1/\tau_{\rm esc}\gamma$. In addition, the impedance shows a low-pass filte due to the influenc of τ_0.

$$H(\omega) = \frac{\omega_r^2\tau_p}{(1 + j\omega\tau_0)\left[\omega_r^2\left(1 + \dfrac{\varepsilon}{\tau_w G_0'}\right) - \omega^2 + j\omega\gamma\right] + j\omega\dfrac{\tau_0}{\tau_{\rm esc}}\left(j\omega + \omega_r^2\dfrac{\varepsilon}{G_0'}\right)}$$

$$Z_i(\omega) = R_c \frac{\omega_r^2\left(1 + \dfrac{\varepsilon}{\tau_w G_0'} + \dfrac{\varepsilon}{\tau_{\rm esc} G_0'}\right) - \omega^2 + j\omega\gamma_I}{(1 + j\omega\tau_0)\left[\omega_r^2\left(1 + \dfrac{\varepsilon}{\tau_w G_0'}\right) - \omega^2 + j\omega\gamma\right] + j\omega\dfrac{\tau_0}{\tau_{\rm esc}}\left(j\omega + \omega_r^2\dfrac{\varepsilon}{G_0'}\right)} \tag{10}$$

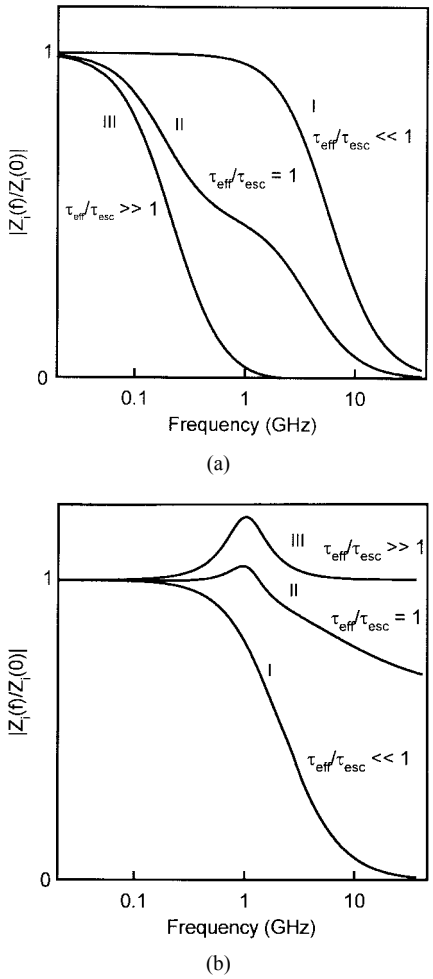

Fig. 3. Magnitude of the normalized impedance,= $|Z_i(f)/Z_i(0)|$ versus frequency f (a) below and (b) above threshold for three different cases of the ratio $\tau_{\rm eff}/\tau_{\rm esc}$. The parameters used were $\tau_{\rm eff} = 1$ ns and $\tau_0 = 35$ ps.

Equation (13) predicts a drop in the intrinsic differential diode resistance at lasing threshold, given by

$$\frac{R_d(I_0 \to I_{\rm th},\, I_0 < I_{\rm th})}{R_d(I_0 \to I_{\rm th},\, I_0 > I_{\rm th})} = 1 + \frac{\tau_{\rm eff}}{\tau_{\rm esc}}. \tag{16}$$

In this case, the ratio $\tau_{\rm eff}/\tau_{\rm esc}$ can be estimated from measured values of the differential diode resistance.

3) Case III—$\eta \ll 1$ and $\tau_{\rm esc} \ll \tau_{\rm eff}$: In this case, the pole at τ_0 and the zero are both at high frequencies, thus the pole at $\tau_{\rm eff}$ dominates the frequency-dependent impedance below threshold. Above threshold, there is a pronounced peak at the relaxation frequency. The intrinsic differential diode resistance exhibits a large drop at threshold and vanishes above threshold due to clamping of the carrier number in the core above threshold. In this case, the behavior of R_d is the same as for ideal bulk lasers, in which the carrier number in the *active region* is clamped above threshold [32]. Taking into account the influenc of R_ϵ and assuming nonperfect gain clamping, the intrinsic differential resistance takes on a small but finit value.

In the case of general values of η, the dynamic behavior becomes far more complicated. However, it is instructive to study the influenc of η on the dynamical properties in the case $\omega\tau_{\rm cap} \ll 1$. In this case, R_c vanishes, and the small-signal intrinsic equivalent circuit of Fig. 2 simplifie to the equivalent circuit shown in Fig. 4(b) with $C_w = \tau_{\rm eff} I_0/mV_T$, $R_w = \tau_{\rm eff}/C_w$, and $C_c = \eta C_w$, with vanishing elements L_w and R_ϵ below threshold and $C_w = \tau_{\rm eff} I_{\rm th}/mV_T$ and $R_w = \tau_w/C_w$ above threshold. The intrinsic impedance below threshold is then given as

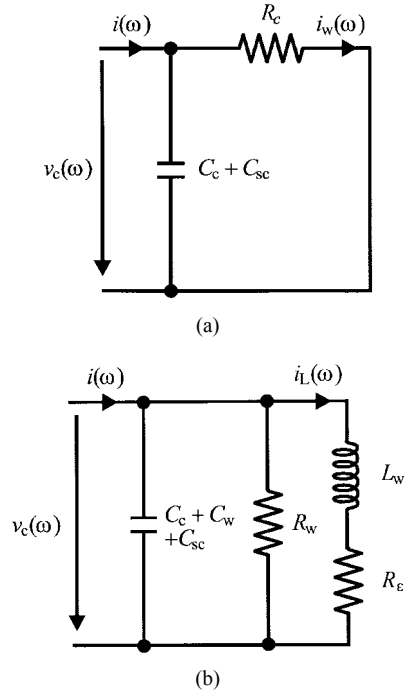

Fig. 4. Small-signal intrinsic equivalent circuit of a QW laser diode in the cases (a) $\eta \ll 1$ and $\tau_{\rm esc} \gg \tau_{\rm eff}$ and (b) $\omega\tau_{\rm cap} \ll 1$.

$$Z_i(\omega) = R_d \frac{1}{1 + j\omega((1+\eta)\tau_{\rm eff} + R_d C_{sc})} \tag{17}$$

with

$$R_d = \frac{mV_T}{I_0}.$$

The expression for the impedance in this case is similar to that of an ideal bulk laser, but with the time constant $(1+\eta)\tau_{\rm eff}$ due to the additional contribution of the unconfine carriers in the core. This case was previously considered in [33]. Above threshold, the modulation response and the intrinsic impedance are given as

$$H(\omega) = \frac{\omega_{r,\,\rm eff}^2}{\omega_{r,\,\rm eff}^2 - \omega^2 + j\omega\gamma_{\rm eff}}$$

and

$$Z_i(\omega) = \omega_{r,\,\rm eff}^2 \frac{R_\varepsilon + j\omega L_w}{\omega_{r,\,\rm eff}^2 - \omega^2 + j\omega\gamma_{\rm eff}} \tag{18}$$

where the effective angular relaxation frequency $\omega_{r,\,\rm eff}$ and the effective damping rate $\gamma_{\rm eff}$ are given by

$$\begin{aligned} \omega_{r,\,\rm eff} &= \frac{\omega_r}{\sqrt{1+\eta+C_{sc}/C_w}} \\ \gamma_{\rm eff} &= \frac{1}{\tau_{\rm eff}(1+\eta+C_{sc}/C_w)} \\ &\quad + \omega_{r,\,\rm eff}^2 \left(\tau_p + \frac{\varepsilon(1+\eta+C_{sc}/C_w)}{G_0'}\right). \end{aligned} \tag{19}$$

TABLE I
STRUCTURAL AND MATERIAL PARAMETERS FOR THE THREE LASER STRUCTURES ANALYZED

Structure No.	Structure	QWs	Barriers	Core	Cladding	V_b(e-) (eV)	V_b(h) (eV)	Doping (cm^{-3})	Ref.
1	p-doped $In_{0.35}Ga_{0.65}As$ MQW	4x5.7 nm $In_{0.35}Ga_{0.65}As$	20 nm GaAs	162 nm GaAs	$Al_{0.8}Ga_{0.2}As$	0.145	0.129	–	[24]
2	undoped $In_{0.35}Ga_{0.65}As$ MQW	4x5.7 nm $In_{0.35}Ga_{0.65}As$	20 nm GaAs	162 nm GaAs	$Al_{0.8}Ga_{0.2}As$	0.145	0.129	$2x10^{19}$ cm^{-3}Be	[24]
3	undoped $In_{0.25}Ga_{0.75}As$ MQW	3x7 nm $In_{0.25}Ga_{0.75}As$	17 nm GaAs	200 nm GaAs	$Al_{0.6}Ga_{0.4}As$	0.108	0.093	–	[34]

In this case, the intrinsic impedance takes on a very low value at zero frequency, vanishing in the case of $\varepsilon = 0$, and has a pronounced peak at the relaxation frequency. Note that, in the usual case $C_{sc}/C_w \ll 1$, the effective relaxation frequency is lower than the intrinsic value ω_r and the effective damping rate is higher than the intrinsic value γ, if the condition $\eta \ll 1$ does not hold. Both effects degrade the modulation response, lowering the maximum achievable modulation bandwidth and the modulation bandwidth at a given bias current. In the limit $\eta \ll 1$, (19) reduces to the corresponding expression for bulk laser diodes.

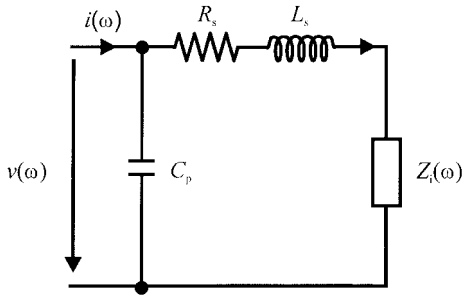

Fig. 5. Equivalent circuit of a mesa diode laser.

VI. EXPERIMENTAL RESULTS

In this section, we present the results of measurements of the frequency-dependent electrical impedance of high-speed laser diodes. Along with the discussion of the measured curves, we present the main parameters extracted by fittin the theoretical expressions of the electrical impedance derived in Section IV to the measured curves.

A. Epilayer and Laser Structures

In the following, we discuss the results of measurements performed on InGaAs–GaAs lasers fabricated from different epilayer structures with a common lateral mesa structure. Structure 1 (p-doped $In_{0.35}Ga_{0.65}As$ MQW) and structure 2 (undoped $In_{0.35}Ga_{0.65}As$ MQW) consist of four 5.7-nm $In_{0.35}Ga_{0.65}As$–GaAs QW's separated by 20-nm GaAs barriers, upper and lower 48-nm-thick GaAs confinemen layers, and $Al_{0.8}Ga_{0.2}As$ cladding layers. Further details of these structures are reported in [24]. Structure 3 (undoped $In_{0.25}Ga_{0.75}As$ MQW) contains three 7-nm $In_{0.25}Ga_{0.75}As$ QW's in a 178-nm-thick GaAs core region and $Al_{0.6}Ga_{0.4}As$ cladding layers [34]. The properties of these three epilayer structures are summarized in Table I with $V_b(e)$ and $V_b(h)$ denoting the barrier height for the confine electrons and holes in the firs QW energy level, respectively (calculated assuming parabolic subbands and 60% of the total band offset in the conduction band). All devices were fabricated in a triple mesa structure [35] with mesa widths in the range of $w = 3$–40 μm, suitable for direct on-wafer probing, and cleaved to lengths of 200–900 μm. For the mesa structure, the parasitics entering into the laser equivalent circuit are the series resistance R_s, originating from the finit conductance of the cladding layers and from the metal–semiconductor contacts, a parallel capacitance C_p, and a series inductance L_s. Using these elements in conjunction with the intrinsic equivalent circuit derived in Section IV, we obtain the equivalent circuit for mesa laser diodes shown in Fig. 5.

B. Electrical Impedance

The measurements of both magnitude and phase of the frequency-dependent impedance below and above threshold were carried out using an HP 8722A network analyzer fully calibrated up to 40 GHz in conjunction with an on-wafer measurement setup. If not otherwise stated, all the measurements were performed at 25 °C.

Fig. 6 shows the measured magnitude of the frequency-dependent impedance $|Z(f)|$ for 3×200 μm^2 lasers fabricated from various structures for different bias currents. A distinct behavior can be clearly observed, coincident with cases I–III in Fig. 3. Below threshold, the impedance of the p-doped $In_{0.35}Ga_{0.65}As$ MQW laser has one real pole with a cut-off frequency exceeding 1 GHz [Fig. 6(a), case I]. The impedance of the undoped $In_{0.35}Ga_{0.65}As$ MQW laser shows two real poles and a real zero [Fig. 6(b), case II]. The impedance of the undoped $In_{0.25}Ga_{0.75}As$ MQW device again has one real pole, but at a much lower cut-off frequency [Fig. 6(c), case III]. Above threshold, the p-doped $In_{0.35}Ga_{0.65}As$ MQW laser has, again, a real pole in the frequency-dependent impedance [Fig. 6(d), case I], whereas the curves of the undoped $In_{0.35}Ga_{0.65}As$ [Fig. 6(e), case II] and the undoped $In_{0.25}Ga_{0.75}As$ MQW lasers [Fig. 6(f), case III] show a resonance peak at the relaxation frequency.

These three different behaviors of the differential diode resistance and of the frequency-dependent impedance correspond to the three cases described in Section V for differ-

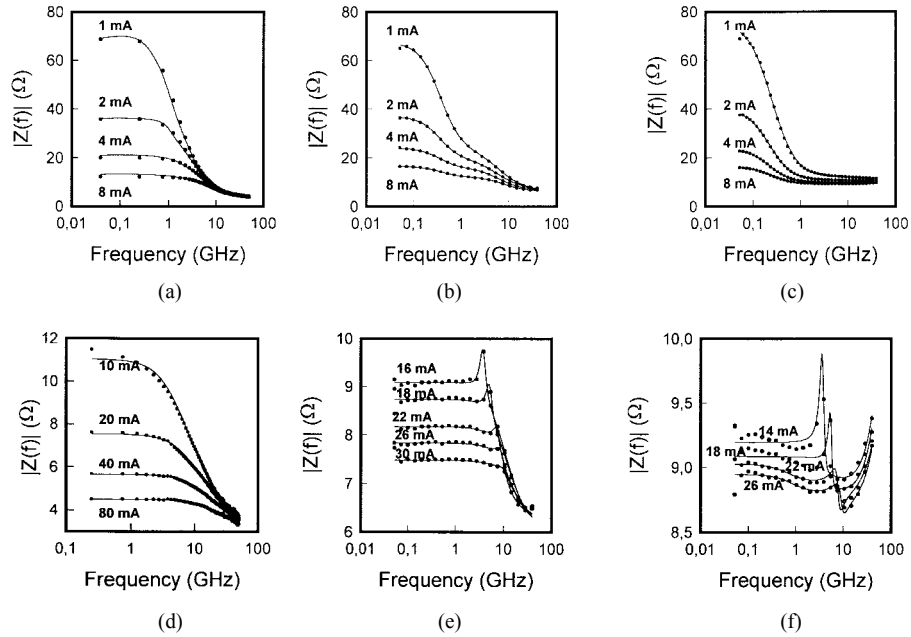

Fig. 6. Measured (points) and fitte (lines) values of the magnitude of the impedance $|Z(f)|$ versus frequency f for 3×200 μm^2 (a)–(c) below and (d)-(f) above threshold with the bias current I_0 as the parameter. (a), (d) A p-doped $In_{0.35}Ga_{0.65}As$ laser. (b), (e) An undoped $In_{0.35}Ga_{0.65}As$ laser. (c), (f) An undoped $In_{0.25}Ga_{0.75}As$ MQW laser.

ent values of the ratio $\tau_{\rm esc}/\tau_{\rm eff}$, with $\tau_{\rm esc}/\tau_{\rm eff}$ much higher than, comparable to, and much lower than unity for devices fabricated from structures 1–3, respectively. The physical origin of the differences in $\tau_{\rm esc}/\tau_{\rm eff}$ arises from the epilayer structure and can be qualitatively understood by considering the expected dependencies of $\tau_{\rm eff}$ on the doping level and of $\tau_{\rm esc}$ on the barrier height: $\tau_{\rm eff}$ decreases with the addition of p-doping in the active region, and $\tau_{\rm esc}$ increases with the barrier height. The active layer of structure 3 is $In_{0.25}Ga_{0.75}As$, and, therefore, the barrier height is lower than in structures 1 and 2 with $In_{0.35}Ga_{0.65}As$ active regions. As a consequence, $\tau_{\rm esc}$ (undoped $In_{0.25}Ga_{0.75}As$ MQW) $\ll \tau_{\rm esc}$ (undoped $In_{0.35}Ga_{0.65}As$ MQW). Since $\tau_{\rm eff}$ is only slightly dependent on the active region material, the ratio $\tau_{\rm esc}/\tau_{\rm eff}$ is much lower than unity for the undoped $In_{0.25}Ga_{0.75}As$ MQW devices and comparable to unity for the undoped $In_{0.35}Ga_{0.65}As$ MQW devices. In the case of the p-doped $In_{0.35}Ga_{0.65}As$ MQW devices, the addition of p-doping to the active region simultaneously produces two effects: it decreases $\tau_{\rm eff}$ ($\tau_{\rm eff}^{-1}$ in doped devices is proportional to $B\tilde{n}_w(\tilde{n}_w+p_0)$ with the QW carrier density $\tilde{n}_w$, the bimolecular radiative recombination constant B, and the p-doping concentration p_o) and it increases $\tau_{\rm esc}$ (see Section VI-E), yielding $\tau_{\rm esc} \gg \tau_{\rm eff}$.

The *exact* small-signal solutions of the rate equations (10) in conjunction with the parasitic circuit elements in Fig. 5 were fitte to the values of both magnitude and phase of the frequency-dependent impedance of lasers with various cavity widths and lengths. Below threshold, the fittin parameters were the dynamic time constants (τ_o for p-doped $In_{0.35}Ga_{0.65}As$ MQW lasers, $\tau_{\rm esc}$, $\tau_{\rm eff}$, and τ_0 for undoped $In_{0.35}Ga_{0.65}As$ MQW lasers, and $\tau_{\rm eff}$ for undoped $In_{0.25}Ga_{0.75}As$ MQW lasers), as well as R_d and the electrical parasitics. As can be observed from the lines in Fig. 6, the fittin quality at frequencies lower than 20 GHz was very good. Above threshold, the values of R_d were too small to obtain reliable values for all the involved parameters: only τ_0, R_d, R_s, and, in some cases, the relaxation frequency could be accurately determined.

C. Differential Diode Resistance

In Fig. 7, we plot the measured $(R_d+R_s)\times I_0/kT$ versus bias current I_0 for 3×200 μm^2 p-doped $In_{0.35}Ga_{0.65}As$, undoped $In_{0.35}Ga_{0.65}As$, and undoped $In_{0.25}Ga_{0.75}As$ MQW devices. These characteristics present three qualitatively different behaviors originated from different values of the ratio $\tau_{\rm eff}/\tau_{\rm esc}$. For the p-doped sample, no drop is observed at threshold, implying $\tau_{\rm esc} \gg \tau_{\rm eff}$ (case I in Section V). Thus, $\tau_{\rm esc}$ cannot be directly determined from these curves. However, we can estimate a lower limit for $\tau_{\rm esc}$ considering the value of $\tau_{\rm eff}$ extracted from the modulation response of the spontaneous emission [36]. These measurements were performed on the p-doped devices [37], and we obtained values of typically 0.2 ns, yielding a lower limit for $\tau_{\rm esc}$ of roughly 2 ns. In contrast, in both the undoped $In_{0.35}Ga_{0.65}As$ and $In_{0.25}Ga_{0.75}As$ MQW samples, a drop in R_d is observed at threshold. From the values slightly below and above threshold of the undoped $In_{0.35}Ga_{0.65}As$ MQW device, the escape time can be estimated, yielding $\tau_{\rm esc} \approx \tau_{\rm eff}$ (case II). For the undoped $In_{0.25}Ga_{0.75}As$ device, the value of R_d above threshold drops to a very small value, yielding $\tau_{\rm esc} \ll \tau_{\rm eff}$ (case III). Below threshold, the values of R_d for all samples present a dependence $R_d = mV_T/I_0$with $m \approx 2.7$ for p-doped and undoped $In_{0.35}Ga_{0.65}As$ devices and $m \approx 2.0$ for undoped $In_{0.25}Ga_{0.75}As$ devices, respectively.

D. Carrier Lifetime

In order to check the validity of the impedance technique to obtain reliable dynamical laser parameters, we compare the

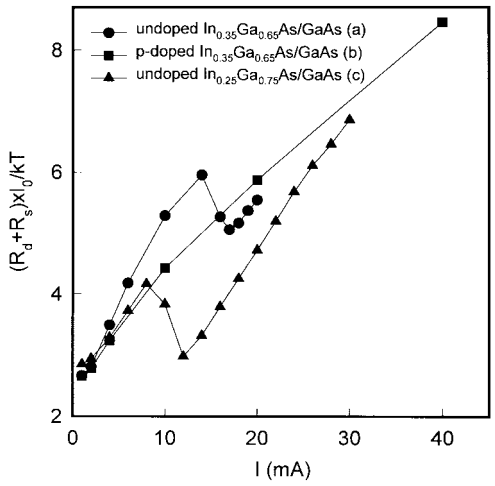

Fig. 7. $(R_d + R_s) \times I_0/kT$ versus bias current I_0 for (a) undoped $In_{0.35}Ga_{0.65}As$, (b) p-doped $In_{0.35}Ga_{0.65}As$, and (c) undoped $In_{0.25}Ga_{0.75}As$ MQW lasers.

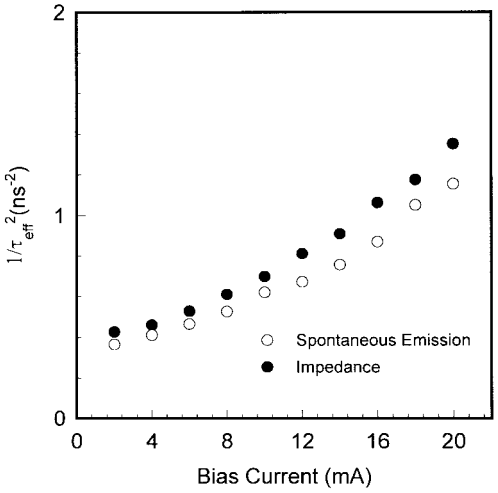

Fig. 8. Comparison of the values of the effective lifetime of carriers in the QW's τ_{eff} versus bias current, as extracted from measurements of the impedance versus frequency (fille symbols) and the modulation of the spontaneous emission versus frequency (open symbols), for a 16×200 μm^2 undoped $In_{0.35}Ga_{0.65}As$ MQW laser below threshold.

extracted values of τ_{eff} for undoped $In_{0.35}Ga_{0.65}As$ MQW lasers with the values obtained from the modulation response of the spontaneous emission measured simultaneously for the same device [37] in Fig. 8. The discrepancy between both sets of values is attributed to the nonuniformity of the lateral carrier profil caused by surface recombination at the external mesa sidewalls [38]. Nevertheless, the discrepancy is small enough to consider the impedance technique as a valid method to determine the effective carrier lifetime in QW lasers. The observed dependence of τ_{eff} on the injection level and mesa width has been analyzed in [37].

E. Escape Time

Fig. 9 shows τ_{esc} for undoped $In_{0.35}Ga_{0.65}As$ MQW lasers with different mesa widths as a function of the carrier density

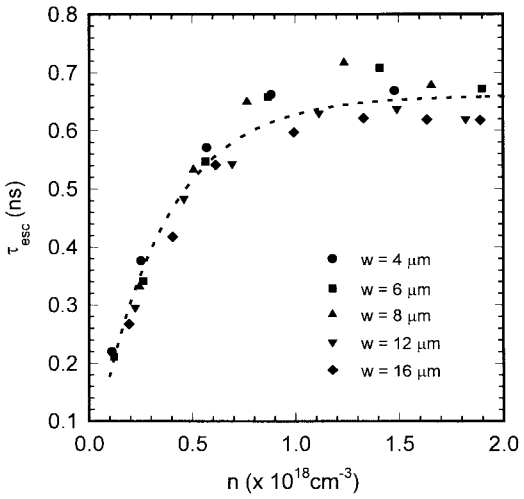

Fig. 9. Carrier escape time τ_{esc} versus QW carrier density for undoped $In_{0.35}Ga_{0.65}As$ MQW lasers with different cavity widths. The line is drawn as a visual aid.

in the QW's. The relation between the steady-state carrier density in the QW's N_{w0}/Ad_w and the bias current was derived using

$$N_{w0}(I_0)/Ad_w = \frac{1}{qAd_w} \int_0^I \tau_{\text{eff}}(I')\, dI' \qquad (20)$$

obtained from (5) in the case of a bias-dependent τ_{eff}. The experimental points lie on a single curve within experimental error, indicating that the extracted τ_{esc} for a given layer structure depends only on the injection level and not on the device dimensions. The same conclusion was obtained by comparing the escape times for lasers with different lateral confinemen structures (mesa or ridge waveguide). The extracted values of τ_{esc} for undoped $In_{0.35}Ga_{0.65}As$ MQW devices increase with carrier density up to a saturation value of ≈0.7 ns. In the case of p-doped $In_{0.35}Ga_{0.65}As$ and undoped $In_{0.25}Ga_{0.75}As$ MQW samples, τ_{esc} cannot be directly determined from the fi of the theoretical impedance to the experimental results, but the absence of a clear zero in the impedance curves in Fig. 6 indicates an upper or lower limit: $\tau_{\text{esc}} \gg 0.2$ ns for a p-doped $In_{0.35}Ga_{0.65}As$ MQW and $\tau_{\text{esc}} \ll 1$ ns for undoped $In_{0.25}Ga_{0.75}As$ MQW devices. A more detailed characterization in terms of τ_{esc} of the above samples and of other laser devices with different epitaxial structures was presented in [15].

The validity of the model can be further checked by investigating the temperature dependence of the escape time. As an example, Fig. 10 shows the values of the magnitude of the electrical impedance normalized to the zero-frequency value for an undoped $In_{0.35}Ga_{0.65}As$ MQW sample at a bias current of 4 mA at various heat-sink temperatures T in the range of 10 °–85 °C. The inset of this figur shows an Arrhenius plot of τ_{esc} at a QW carrier density of 5.2×10^{17} cm^{-3} versus $1/kT$. We have analyzed the temperature dependence of τ_{esc} at a constant injected carrier density and not at a constant injection current, but the differences between both approaches are not

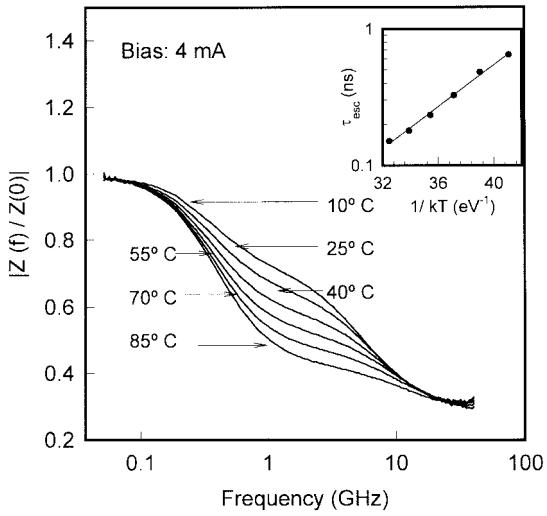

Fig. 10. Magnitude of the normalized impedance versus frequency at different temperatures for a 4×200 μm^2 undoped $In_{0.35}Ga_{0.65}As$ MQW laser. The inset shows the carrier escape time τ_{esc} versus inverse temperature at a constant carrier density of 5.2×10^{17} cm^{-3}.

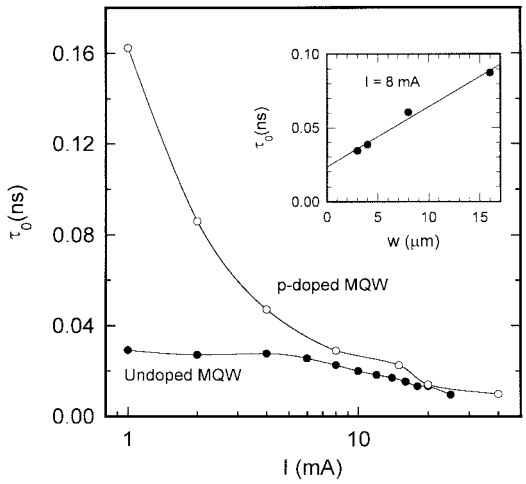

Fig. 11. Values of the electrical diode time constant τ_0 as extracted from the measured values of the impedance versus frequency, for 3×200 μm^2 p-doped $In_{0.35}Ga_{0.65}As$ and undoped $In_{0.35}Ga_{0.65}As$ lasers. The inset shows the values of τ_0 at $I_0 = 8$ mA versus the mesa width w for p-doped $In_{0.35}Ga_{0.65}As$ devices.

significant The extracted escape times can be approximated by

$$\tau_{\rm esc}(N_w, T) = \tau_{\rm esc0}(N_w)\,\exp\left(\frac{E_a}{kT}\right) \qquad (21)$$

where $E_a = 0.17\pm0.02$ eV. Considering the small temperature range and the experimental error, the extracted values of E_a are in reasonable agreement with the electron barrier height of 0.145 eV, as predicted by thermionic emission theory [39].

The extracted values for $\tau_{\rm esc}$ are more than one order of magnitude higher than those theoretically calculated considering carrier–polar longitudinal optical phonon interactions [40]. The observed increase of $\tau_{\rm esc}$ with the p-doping concentration and the carrier density dependence in the case of undoped $In_{0.35}Ga_{0.65}As$ MQW lasers are attributed to the combination of different effects: 1) an increase of the effective electron barrier height caused by the band-bending in the p-doped structures; 2) band-fillin at high injection levels; 3) carrier-induced bandgap narrowing; and 4) a residual and nonuniform p-doping profil in the case of nominally undoped $In_{0.35}Ga_{0.65}As$ structures [41]. A detailed analysis relating the measured escape times and its bias and temperature dependencies on the epilayer structure is beyond the scope of this paper; theoretical calculations considering the above described physical effects can be found in [42] and [43].

F. Diode Time Constant

Fig. 11 presents the values of the electrical diode time constant τ_0 as a function of the bias current for 3×200 μm^2 p-doped and undoped $In_{0.35}Ga_{0.65}As$ MQW lasers. The dependencies are well understood considering (12): the electrical time constant is given by the sum of the capture time and the term $R_cC_{\rm sc}$ associated with the space–charge capacitance. Below threshold, the latter term is inversely proportional to the bias current, due to the dependence $R_c \sim I^{-1}$, if we neglect the weak dependence of $C_{\rm sc}$ on I. Since this term vanishes at high bias currents, an estimate for $\tau_{\rm cap}$ can be obtained from the values of τ_0 at high bias currents, yielding values of $\tau_{\rm cap} \sim$ 2–5 ps, corresponding to a physical capture time of $\tau_{\rm cap,\,phys} \sim$ 0.2–0.5 ps for both undoped and p-doped $In_{0.35}Ga_{0.65}As$ MQW lasers. For the undoped $In_{0.25}Ga_{0.75}As$ MQW lasers, the values of τ_0 cannot be extracted from the impedance curves. The increase in τ_0 with doping concentration in the MQW devices is due to the increase of $C_{\rm sc}$ with doping level at a constant voltage [44] in conjunction with the increased influenc of R_c in the expression for τ_0 due to the larger value of $\tau_{\rm esc}$ for the doped devices. In the doped devices, the dominant contribution to τ_0 originates from the space–charge capacitance at low and moderate bias currents, yielding $\tau_0 \propto w$ with the mesa width w. This is confirme in the inset of Fig. 11, where we plotted the values of τ_0 versus w at a fixe bias current of 8 mA.

G. Relaxation Frequency

The measurement of impedance above threshold is an alternative technique to the measurement of the modulation response for the determination of the relaxation frequency f_r and the damping rate γ, in the case $\tau_{\rm esc} < \tau_{\rm eff}$. As an example, we have plotted in Fig. 12 the values of f_r^2 versus bias current for an undoped $In_{0.25}Ga_{0.75}As$ MQW laser. These values present a linear behavior. From the slope of this curve, the differential gain can be extracted, yielding $G_0'/v_g = 0.9\times10^{-15}$ cm^2 with group velocity v_g. This value is lower than the corresponding values of 2.2×10^{-15} cm^2 and 2.5×10^{-15} cm^2 for the undoped and p-doped $In_{0.35}Ga_{0.65}As$ MQW devices, respectively, reported in [24] due to lower In content in the QW's and the higher carrier density per QW.

VII. Conclusion

We have performed measurements of the electrical impedance of InGaAs–GaAs laser diodes fabricated from

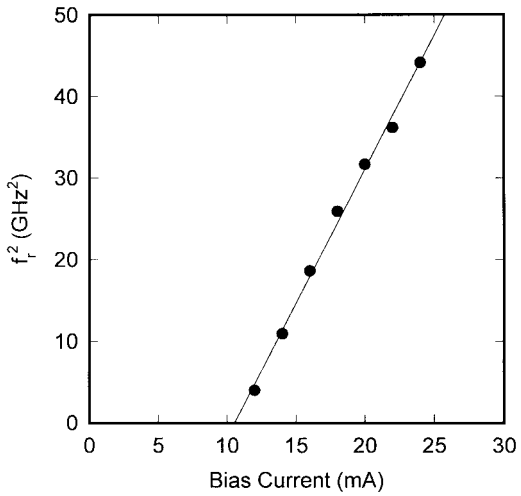

Fig. 12. Values of the squared relaxation frequency f_r^2 as extracted from the measured values of the impedance versus frequency for $3\times200\ \mu\text{m}^2$ undoped $In_{0.25}Ga_{0.75}As$ MQW laser.

different epilayer structures. The results were shown to be in good agreement for all layer structures with the predictions of a three-rate-equation model, which takes into account the influence of carrier capture/transport into and carrier re-emission out of the QW's. Impedance measurements were shown to be a powerful method for extracting the carrier escape time τ_{esc}, which cannot be unambiguously determined using conventional dynamical measurements such as modulation response or RIN measurements. For undoped $In_{0.35}Ga_{0.65}As$ MQW devices, we obtain $\tau_{\text{esc}} \sim 0.7$ ns with a weak bias dependence. In addition, we get an estimate for the physical capture time from these measurements of $\tau_{\text{cap, phys}} \sim 0.2$–$0.5$ ps for undoped and p-doped $In_{0.35}Ga_{0.65}As$ MQW devices. Using these values of τ_{esc} and $\tau_{\text{cap, phys}}$, we conclude that carrier capture and escape does not limit the modulation bandwidth of properly designed InGaAs–GaAs lasers with MQW active regions and narrow confinemen regions. The bandwidth limit in these devices originates from internal damping due to nonlinear gain or power dissipation.

APPENDIX

Linearization of (1) yields (A1), shown at the bottom of the page.

Substitution of $n_c(\omega)$ and $n_w(\omega)$ using (7) and (8) in conjunction with the equivalent circuit elements define in (7)–(9) results in (A2), shown at the bottom of the page, translating into the small-signal equivalent circuit in Fig. 2. The determinant $\Delta(\omega) = \det(A)$ of the rate matrix in (A1) is calculated by replacing the second row by the sum of the second and third rows

$$\Delta(\omega)\tau_{cap} = \det\begin{pmatrix} j\omega + \omega_r^2\dfrac{\varepsilon}{G_0'} & -\omega_r^2\tau_p & 0 \\ \dfrac{1}{\tau_p} & j\omega + \left(\omega_r^2\tau_p + \dfrac{1}{\tau_{\text{eff}}}\right) & j\omega\tau_0 \\ 0 & -\dfrac{1}{\tau_{esc}} & j\omega\tau_0 + 1 \end{pmatrix}. \tag{A3}$$

Evaluation of this determinant yields

$$\begin{aligned}\Delta(\omega)\tau_{\text{cap}} &= (1+j\omega\tau_0)\det\begin{pmatrix} j\omega + \omega_r^2\dfrac{\varepsilon}{G_0'} & -\omega_r^2\tau_p \\ \dfrac{1}{\tau_p} & j\omega + \left(\omega_r^2\tau_p + \dfrac{1}{\tau_{\text{eff}}}\right) \end{pmatrix} \\ &\quad + j\omega\frac{\tau_0}{\tau_{\text{esc}}}\cdot\left(j\omega + \omega_r^2\frac{\varepsilon}{G_0'}\right).\end{aligned} \tag{A4}$$

The 2×2 determinant in (A4) is exactly the denominator of the small-signal transfer function of a bulk laser. Using the expression for the damping rate of a bulk laser, $\gamma = 1/\tau_{\text{eff}} + \omega_r^2(\tau_p + \varepsilon/G_0')$, (A4) simplifie to

$$\begin{aligned}\Delta(\omega)\tau_{\text{cap}} &= (1+j\omega\tau_0)\cdot\left(\omega_r^2\left(1+\frac{\varepsilon}{\tau_w G_0'}\right) - \omega^2 + j\omega\gamma\right) \\ &\quad + j\omega\frac{\tau_0}{\tau_{\text{esc}}}\cdot\left(j\omega + \omega_r^2\frac{\varepsilon}{G_0'}\right).\end{aligned} \tag{A5}$$

ACKNOWLEDGMENT

The authors wish to thank W. Benz, J. Fleissner, B. Matthes, K. Räuber, B. Wieber, M. Maier, R. E. Sah, E. Larkins, J. Arias, K. Czotscher, and M. Mikulla for their assistance with sample preparation and characterization.

$$\begin{pmatrix} j\omega + \omega_r^2\dfrac{\varepsilon}{G_0'} & -\omega_r^2\tau_p & 0 \\ \dfrac{1}{\tau_p} & j\omega + \dfrac{1}{\tau_{\text{eff}}} + \dfrac{1}{\tau_{\text{esc}}} + \omega_r^2\tau_p & -\dfrac{1}{\tau_{cap}} \\ 0 & -\dfrac{1}{\tau_{\text{esc}}} & j\omega\left(1+\dfrac{C_{\text{sc}}}{C_c}\right) + \dfrac{1}{\tau_{\text{cap}}} \end{pmatrix} \cdot \begin{pmatrix} n_p(\omega) \\ n_w(\omega) \\ n_c(\omega) \end{pmatrix} = \begin{pmatrix} 0 \\ 0 \\ \frac{i(\omega)}{q} \end{pmatrix} \tag{A1}$$

$$\begin{pmatrix} j\omega L_w + R_e & -1 & 0 \\ 1 & j\omega C_w + R_w^{-1} + R_c^{-1} & -R_c^{-1} \\ 0 & -R_c^{-1} & j\omega(C_c + C_{\text{sc}}) + R_c^{-1} \end{pmatrix} \cdot \begin{pmatrix} i_L(\omega) \\ v_w(\omega) \\ v_c(\omega) \end{pmatrix} = \begin{pmatrix} 0 \\ 0 \\ i(\omega) \end{pmatrix} \tag{A2}$$

REFERENCES

[1] Y. Arakawa and A. Yariv, "Theory of gain, modulation response, and spectral linewidth in AlGaAs quantum well lasers," *IEEE J. Quantum Electron.,* vol. QE-21, pp. 1666–1674, 1985.

[2] I. Suemune, L. A. Coldren, M. Yamanishi, and Y. Kan, "Extremely wide modulation bandwidth in a low threshold current strained quantum well laser," *Appl. Phys. Lett.,* vol. 53, pp. 1378–1380, 1988.

[3] Y. Matsui, H. Murai, S. Arahira, S. Kutsuzawa, and Y. Ogawa, "30 GHz bandwidth 1.55 μm strain-compensated InGaAlAs/InGaAsP MQW laser," *IEEE Photon. Technol. Lett.,* vol. 9, pp. 25–27, 1997.

[4] O. Kjebon, R. Schatz, S. Lourdudoss, S. Nilsson, J. Stalnacke, and L. Bäckbom, "30 GHz direct modulation bandwidth in detuned loaded InGaAsP DBR lasers at 1,55 μm wavelength," *Electron. Lett.,* vol. 33, pp. 488–489, 1997.

[5] S. Weisser, E. C. Larkins, K. Czotscher, W. Benz, I. Daleiden, I. Esquivias, J. Fleissner, J. D. Ralston, B. Romero, R. E. Sah, A. Schönfelder, and J. Rosenzweig, "Damping-limited modulation bandwidths up to 40 GHz in undoped short-cavity $In_{0.35}Ga_{0.65}As$–GaAs multiple-quantum-well lasers," *IEEE Photon. Technol. Lett.,* vol. 8, pp. 608–610, 1996.

[6] X. Zhang, A. L. Gutierrez-Aitken, D. Klotzkin, P. Bhattacharya, C. Caneau, and R. Bhat, "0.98 μm multiquantum well tunnelling injection lasers with ultra-high modulation bandwidths," *Electron. Lett.,* vol. 32, pp. 1715–1717, 1996.

[7] R. Nagarajan, M. Ishikawa, T. Fukushima, R. S. Geels, and J. E. Bowers, "High speed quantum-well lasers and carrier transport effects," *IEEE J. Quantum Electron.,* vol. 28, pp. 1990–2008, 1992.

[8] M. O. Vassell, W. F. Sharfin W. C. Rideout, and J. Lee, "Competing effects of well-barrier hole burning and nonlinear gain on the resonance characteristics of quantum-well lasers," *IEEE J. Quantum Electron.,* vol. 29, pp. 1319–1329, 1993.

[9] T. C. Wu, S. C. Kan, D. Vassilovski, K. Y. Lau, C. E. Zah, B. Pathak, and T. P. Lee, "Gain compression in tensile strained 1.55 μm quantum well lasers operating at firs and second quantized states," *Appl. Phys. Lett.,* vol. 60, pp. 1794–1796, 1992.

[10] N. Tessler, R. Nagar, and G. Eisenstein, "Structure dependent modulation responses in quantum-well lasers," *IEEE J. Quantum Electron.,* vol. 28, pp. 2242–2250, 1992.

[11] R. Nagarajan, M. Ishikawa, and J. E. Bowers, "Effects of carrier transport on relative intensity noise and critique of K factor predictions of modulation response," *Electron. Lett.,* vol. 28, pp. 846–848, 1992.

[12] S. Weisser, I. Esquivias, P. J. Tasker, J. D. Ralston, B. Romero, and J. Rosenzweig, "Impedance characteristics of quantum-well lasers," *IEEE Photon. Technol. Lett.,* vol. 12, pp. 1421–1423, 1994.

[13] S. Weisser, I. Esquivias, P. J. Tasker, J. D. Ralston, and J. Rosenzweig, "Impedance, modulation response, and equivalent circuit of ultra-high-speed $In_{0.35}Ga_{0.65}As$/GaAs MQW lasers with p-doping," *IEEE Photon. Technol. Lett.,* vol. 6, pp. 782–785, 1994.

[14] I. Esquivias, S. Weisser, B. Romero, J. D. Ralston, and J. Rosenzweig, "Carrier capture and escape times in $In_{0.35}Ga_{0.65}As$/GaAs multi-quantum well lasers determined from high-frequency electrical impedance measurements," *IEEE Photon. Technol. Lett.,* vol. 8, pp. 1294–1296, 1996.

[15] I. Esquivias, B. Romero, S. Weisser, K. Czotscher, J. D. Ralston, E. C. Larkins, J. Arias, A. Schönfelder, M. Mikulla, J. Fleissner, and J. Rosenzweig, "Carrier escape time in GaAs/AlGaAs and InGaAs/GaAs quantum-well lasers," *Proc. SPIE,* vol. 2684, pp. 17–26, 1996.

[16] D. Klotzkin, X. Zhang, P. Bhattacharya, C. Caneau, and R. Bhat, "Carrier dynamics in high-speed ($f_{3\mathrm{dB}} > 40$ GHz) 0.98 μm multiquantum-well tunneling injection lasers determined from electrical impedance measurements," *IEEE Photon. Technol. Lett.,* vol. 9, pp. 578–580, 1997.

[17] H. Hirayama, J. Yoshida, Y. Miyake, and M. Asada, "Carrier capture time and its effect on the efficienc of quantum-well lasers," *IEEE J. Quantum Electron.,* vol. 30, pp. 54–62, 1994.

[18] R. Nagarajan, T. Fukushima, S. W. Corzine, and J. E. Bowers, "Effects of carrier transport on high-speed quantum well lasers," *Appl. Phys. Lett.,* vol. 59, pp. 1835–1837, 1991.

[19] R. S. Tucker and D. J. Pope, "Circuit modeling of the effect of diffusion on damping in a narrow-stripe semiconductor laser," *IEEE J. Quantum Electron.,* vol. QE-19, pp. 1179–1183, 1983.

[20] ———, "Microwave circuit models of semiconductor injection lasers," *IEEE Trans. Microwave Theory Tech.,* vol. MTT-31, pp. 289–294, 1983.

[21] R. Nagarajan and J. E. Bowers, "Effects of carrier transport on injection efficienc and wavelength chirping in quantum-well lasers," *IEEE J. Quantum Electron.,* vol. 29, pp. 1601–1608, 1993.

[22] S. C. Kan, D. Vassilovski, T. C. Wu, and K. Y. Lau, "Quantum capture limited modulation bandwidth of quantum well, wire, and dot lasers," *Appl. Phys. Lett.,* vol. 62, pp. 2307–2309, 1993.

[23] S. C. Kan, D. Vassilovski, T. C. Wu, and K. Y. Lau, "On the effects of carrier diffusion and quantum capture in high speed modulation of quantum well lasers," *Appl. Phys. Lett.,* vol. 61, pp. 752–754, 1992.

[24] J. D. Ralston, S. Weisser, I. Esquivias, E. C. Larkins, J. Rosenzweig, P. J. Tasker, and J. Fleissner, "Control of differential gain, nonlinear gain, and damping factor for high-speed applications of GaAs-based MQW lasers," *IEEE J. Quantum Electron.,* vol. 29, pp. 1648–1659, 1993.

[25] J. Lee, M. O. Vassel, and G. J. Jan, "Energy-band diagrams of P-i-N heterostructures for single quantum-well lasers," *IEEE J. Quantum Electron.,* vol. 29, pp. 1469–1476, 1993.

[26] C. S. Harder, B. J. Van Zeghbroeck, M. P. Kesler, H. P. Meier, P. Vettiger, D. J. Webb, and P. Wolf, "High-speed GaAs/AlGaAs optoelectronic devices for computer applications," *IBM J. Res. Develop.,* vol. 34, pp. 568–583, 1990.

[27] N T. C. Wu, D. Vassiloski, D. M. Cutrer, S. C. Kan, and K. Lau, "Spontaneous emission measurements for resolving damping mechanisms in direct modulation of quantum well lasers," *Appl. Phys. Lett.,* vol. 69, pp. 1050–1052, 1996.

[28] M. Morishita, T. Ohmi, and J.-I. Nishizawa, "Impedance characteristics of double-hetero structure laser diodes," *Solid-State Electron.,* vol. 22, pp. 951–962, 1979.

[29] J. Katz, S. Margalit, C. Harder, D. Wilt, and A. Yariv, "The intrinsic electrical equivalent circuit of a laser diode," *IEEE J. Quantum Electron.,* vol. QE-17, pp. 4–7, 1981.

[30] S. C. Kan and K. Y. Lau, "Intrinsic equivalent circuit of quantum-well lasers," *IEEE Photon. Technol. Lett.,* vol. 4, pp. 528–530, 1992.

[31] M. F. Lu, J. S. Deng, C. Juang, M. J. Jou, and J. B. Lee, "Equivalent circuit model of quantum-well lasers," *IEEE J. Quantum Electron.,* vol. 31, pp. 1418–1422, 1995.

[32] W. B. Joyce and R. W. Dixon, "Electrical characterization of heterostructure lasers," *J. Appl. Phys.,* vol. 49, pp. 3719–3728, 1978.

[33] T. Odagawa, K. Nakajima, K. Tanaka, H. Nobuhara, T. Inoue, N. Okazaki, and K. Wakao, "Separate-confinemen heterostructure dependence of the effective carrier recombination coefficien of strained InGaAs/InGaAsP multiple quantum well lasers," *Appl. Phys. Lett.,* vol. 63, pp. 2996–2998, 1993.

[34] M. Mikulla, W. Benz, P. Chazan, J. Daleiden, J. Fleissner, G. Kaufel, E. C. Larkins, M. Maier, J. D. Ralston, J. Rosenzweig, and A. Wetzel, "High-power tapered InGaAs/GaAs laser diodes with carbon doped cladding layers grown by solid source molecular beam epitaxy," in *Proc. 22nd Int. Symp. Compound Semiconductors*, 1995, Korea, vol. 145, pp. 995–998.

[35] S. D. Offsey, W. J. Schaff, P. J. Tasker, and L. F. Eastman, "Optical and microwave performance of GaAs–AlGaAs and strained-layer InGaAs–GaAs–AlGaAs graded index separate confinemen heterostructure single quantum well lasers," *IEEE Photon. Technol. Lett.,* vol. 2, pp. 9–11, 1990.

[36] R. Olshansky, C. B. Su, J. Manning, and W. Powazinik, "Measurement of radiative and nonradiative recombination rates in InGaAsP and AlGaAs light sources," *IEEE J. Quantum Electron.,* vol. QE-20, pp. 838–854, 1984.

[37] K. Czotscher, S. Weisser, E. C. Larkins, J. Fleissner, J. D. Ralston, A. Schönfelder, J. Rosenzweig, and I. Esquivias, "Structural and carrier density dependence of carrier lifetime in InGaAs/GaAs multiple-quantum-well lasers," *Appl. Phys. Lett.,* vol. 69, pp. 3158–3160, 1996.

[38] M. S. Torre, I. Esquivias, B, Romero, K. Czotscher, S. Weisser, J. D. Ralston, E. C. Larkins, W. Benz, and J. Rosenzweig, "Lateral carrier profil for mesa-structured InGaAs/GaAs Lasers," *J. Appl. Phys.,* vol. 81, pp. 6268–6271, 1997.

[39] H. Schneider and K. von Klitzing, "Thermionic emission and Gaussian transport of holes in $GaAs/Al_xGa_{1-x}As$ multiple-quantum-well structure," *Phys. Rev. B,* vol. 38, pp. 6160–6165, 1988.

[40] C. Y. Tsai, C. Y. Tsai, Y. H. Lo, R. M. Spencer, and L. F. Eastman, "Nonlinear gain effects in semiconductor lasers: Effects of carrier diffusion, capture, and escape," *IEEE J. Select. Topics Quantum Electron.,* vol. 1, pp. 316–330, 1995.

[41] J. Arias, I. Esquivias, J. D. Ralston, E. C. Larkins, S. Weisser, J. Rosenzweig, A. Schönfelder, and M. Maier, "Carrier profil for $In_{0.35}Ga_{0.65}As$/GaAs multi-quantum well lasers from capacitance-voltage measurements," *Appl. Phys. Lett.,* vol 68, pp. 1138–1140, 1996.

[42] B. Romero, I. Esquivias, J. Arias, G. Batko, S. Weisser, and J. Rosenzweig, "Carrier escape time in quantum well lasers: Dependence on injection level, doping concentration, and temperature," in *Proc.*

LEOS'97—10th Annu. Meet., San Francisco, CA, Nov. 10–13, 1997, pp. 142–143.
[43] B. Romero, "Análisis teórico y experimental de los efectos de captura y escape de portadores en láseres de pozo cuántico," Ph.D. dissertation, Universidad Politécnica de Madrid, Madrid, Spain, 1998.
[44] S. M. Sze, *Physics of Semiconductor Devices,* 2nd ed. New York: Wiley, 1981.

I. Esquivias (M'94), photograph and biography not available at the time of publication.

S. Weisser, photograph and biography not available at the time of publication.

B. Romero, photograph and biography not available at the time of publication.

J. D. Ralston (M'50–LM'87), photograph and biography not available at the time of publication.

J. Rosenzweig, photograph and biography not available at the time of publication.